Chemical Geology 572 (2021) 120197

Contents lists available at ScienceDirect

Chemical Geology

journal homepage: www.elsevier.com/locate/chemgeo

Temporally variable crustal contributions to primitive mantle-derived Columbia River Basalt Group magmas

James M.D. Day [a,*], Kimberley L.R. Nutt [a], Brendon Mendenhall [a], Bradley J. Peters [a,b]

[a] Scripps Institution of Oceanography, University of California San Diego, La Jolla, CA 92093, USA
[b] Institute for Geochemistry and Petrology, ETH Zürich, 8092 Zürich, Switzerland

ARTICLE INFO

Editor: Balz Kamber

Keywords:
Osmium
Columbia River Basalt Group
Mantle plume
Temporal changes
Climate

ABSTRACT

The Steens Formation is one of the earliest and most primitive (>7 wt. MgO) eruptive products of the Columbia River Basalt Group (CRBG) and the CRBG-Yellowstone-Snake River large igneous province. New major-, trace-, and highly siderophile-element abundance and $^{87}Sr/^{86}Sr$, $^{143}Nd/^{144}Nd$ and $^{187}Os/^{188}Os$ data are reported for the lower and upper Steens Formation to examine likely mantle sources and the nature of magmatic differentiation and crustal contamination acting on lavas. Examined Steens Formation basalts are relatively mafic (7–9 wt% MgO), incompatible trace element enriched, and have weaker Nb and Ta anomalies compared to other CRBG lavas. The most primitive basalts have isotopic compositions at the time of crystallization consistent with originating from a mantle source that was relatively depleted ($^{87}Sr/^{86}Sr = \sim 0.7033$; $\varepsilon_{Nd}i = \sim +6.5$; $\gamma_{Os}i = \sim +1$). Primary magma compositions for the Steens Formation do not provide compelling evidence for a subducted slab component, instead suggesting derivation from primitive mantle sources more similar to those of other Mesozoic continental flood basalts (CFB; e.g., Deccan, North Atlantic Igneous Province). Onset of sulfide saturation in the CRBG occured at lower MgO (<7 wt%) than in other CFB (~ 8 wt%) leading to the high Os contents in the Steens Formation. Collectively, the Steens Formation exhibits decreasing Os contents, $\varepsilon_{Nd}i$ values and increasing $^{187}Os/^{188}Os$ with decreasing MgO. These geochemical signatures are consistent with increasing crustal contamination to parent melts with time, a feature that is also shared for the CRBG as a whole. Calculations based on Os and Nd isotopes of likely mantle and crust components to different formations of the CRBG indicates a progressive increase in the quantities of crustal contamination from ~1 to 2% from Steens Formation magmatism to more than 6% during Grande Ronde and Wanapum eruptions. These results would indicate increasing crustal contamination and enhanced potential cryptic degassing of CO_2 in the later, more voluminous stages of CRBG magmatism, after ~16.5 Ma. Unless mantle-derived melts can produce sufficient greenhouse gas emission, there is likely an offset between the inception of the mid-Miocene Climatic Optimum at 17 Ma and maximum CO_2 release, indicating that CRBG eruption was a contributing factor to climate change at that time, but was not the trigger for it.

1. Introduction

The Columbia River Basalt Group (CRBG) represent a series of basaltic and basaltic andesite lavas that were erupted during a relatively restricted time period in the mid-Miocene (~17 to ~15.9 Ma; Barry et al., 2013; Kasbohm and Schoene, 2018; Cahoon et al., 2020) in the region that is now Oregon, Washington, northern Idaho, and northern Nevada, USA. The CRBG has been shown to have formed essentially without interruption, with broad northward migration of lava emplacement with time that intersects the Yellowstone-Snake River Plain hotspot track and represents the earliest stages of the magmatic province (e.g., Camp et al., 2013). For these reasons, the CRBG is widely recognized as the youngest - but also the smallest - of the world's continental flood basalts (CFB; e.g., Camp et al., 2013). At approximately 210,000 km^3 of erupted volume (Reidel et al., 2013), the CRBG is several factors to an order of magnitude smaller than the ~30 Ma Ethiopian/Yemen CFB (north eastern Africa and the Arabian Peninsula), ~60 Ma North Atlantic Igneous Province (Northern Canada, Greenland, UK), the ~65 Ma Deccan Traps (India), or the 133 Ma Parana-Etendeka CFB (Southern Africa and South America; e.g., Coffin and Eldholm, 1994;

* Corresponding author.
E-mail address: jmdday@ucsd.edu (J.M.D. Day).

https://doi.org/10.1016/j.chemgeo.2021.120197
Received 2 November 2020; Received in revised form 22 March 2021; Accepted 23 March 2021
Available online 26 March 2021

Courtillot and Renne, 2003). These CFB have all been linked to major mantle plume-continental crust impingement events during the Mesozoic and have been widely cited as playing crucial roles in climate change events due to exchange of CO_2 and other greenhouse gases with the atmosphere (Self et al., 2006; Armstrong-McKay et al., 2014; Rampino and Self, 2015; Pernet-Fisher et al., 2017).

The flood basalts forming the CRBG are particularly important for examining the likely mantle and crustal source(s) and role of CFB in affecting Earth's climate. Its youthfulness means that the CRBG formed at a time when higher-precision records of climatic change are available than for other CFB. Eruption of the CRBG roughly coincides with the mid-Miocene Climatic Optimum (15–17 Ma), and has been cited as a possible trigger or major contributor to this climate warming event (e.g., Foster et al., 2012; Armstrong-McKay et al., 2014; Kasbohm and Schoene, 2018). Linked to this issue is the expansive research done to examine the oldest to the youngest basaltic formations of the CRBG, their likely mantle sources, and the role of crustal contamination on their geochemical compositions. A particularly remarkable feature of the CRBG compared with other CFB are the differentiated compositions of the basaltic and basaltic andesite lavas, and the progressive changes in the compositions of long-lived radiogenic isotope systems (Sr, Nd, Pb) to more enriched compositions with time. From the oldest Steens (~17 to 16.4 Ma) and Picture Gorge basalts (~17.2 to 16.1 Ma), to Imnaha (16.6 to 16.5 Ma), Grande Ronde (16.5 to 16.1 Ma), Wanapum (16.1 to 15.9 Ma) and, finally, the Saddle Mountains Basalts (<15.9 Ma; e.g., Barry et al., 2013; Kasbohm and Schoene, 2018; Cahoon et al., 2020), basaltic lavas rarely exceed 7 wt% MgO and tend towards lower $^{143}Nd/^{144}Nd$ and increasing $^{87}Sr/^{86}Sr$ (e.g., Wolff et al., 2008). The temporal geochemical character of CRBG lavas has been debated, with mantle sources including plume-derived materials, depleted mid-ocean ridge basalt mantle and enriched sources, including continental lithosphere all being proposed, with additional, superimposed complex crystallization and contamination effects (e.g., Carlson et al., 1981; Carlson, 1984; Hooper and Hawkesworth, 1993; Brandon et al., 1993; Camp and Hanan, 2008; Wolff et al., 2008; Camp et al., 2013; Moore et al., 2020).

For all of the chronological and geochemical isotope studies performed on the CRBG, these basalts have not been completely characterized for Re-Os isotopes or highly siderophile element (HSE: Os, Ir, Ru, Pt, Pd, Re) abundances. This omission is important since the HSE, and the Re-Os isotope system embedded within them, are robust tracers of crustal assimilation processes acting on magmas, and for determining initial parental melt compositions (Shirey and Walker, 1998; Day, 2013; Gannoun et al., 2016). Previous Re-Os isotope studies have examined strongly differentiated components of the CRBG, including detailed studies of compound lava flows (Chesley and Ruiz, 1998; Vye-Brown et al., 2013). Recently, Re-Os isotope data was also presented for the Steens Formation (Moore et al., 2020). These studies provide a tantalizing glimpse of progressive fractionation of mantle-derived melts in the CRBG that track crustal contamination. Here we present a comprehensive major-, trace-element and HSE abundance and Sr, Nd, Os isotope study of some of the most primitive basalts from the CRBG that are preserved in the Steens Formation (hereafter referred to as either Steens Formation or Steens Basalts). We examine the roles of complex differentiation and crustal assimilation recognized previously (Moore et al., 2018), and use the new data to constrain the mantle sources of CRBG lavas, the quantities of crust assimilated during the eruptive episodes and the implications these results have for geodynamic models of western North America in the mid Miocene, as well as for the mid-Miocene Climatic Optimum.

2. Samples and methods

Samples were collected from the Steens Mountain region during field campaigns in 2014 and 2015, and from the same 'type' transects used by previous studies (Johnson et al., 1998; Camp et al., 2013; Moore et al., 2018). Samples tie to these prior transect analyses through the reported latitude and longitudes, and with absolute height measurements (from the mean sea level datum), independently verified using altimetry and mapping software (Table S1; Fig. S1). For comparison, two Pliocene rocks overlying the Steens Basalt were collected, including the ~9.5 Ma Devine Canyon tuff (Walker, 1990). Also for comparison, Imnaha lava flows proximal to the Steens Mountain were collected. >1 kg blocks were hammered from outcrops with the aim of obtaining the most mafic basalts, unaffected by surficial weathering. Samples were sawn, sanded to remove any sign of metal, and crushed and powdered in alumina, prior to geochemical analyses. Major element compositions were measured by X-ray fluorescence (XRF) at Franklin and Marshall College using a *PW 2404 PANalytical XRF* vacuum spectrometer following the procedures in Boyd and Mertzman, 1987. All other work was performed at the *Scripps Isotope Geochemistry Laboratory* (*SIGL*), Scripps Institution of Oceanography. Trace-element abundances were determined using digestion and preparation methods described previously (Day et al., 2017). Solutions were measured using a *Thermo Scientific* iCAP Qc quadrupole inductively coupled plasma mass spectrometer. Reproducibility and accuracy of standard reference materials was better than 2% (RSD) for major elements and 5% (RSD) for trace elements in both basaltic and peridotite reference materials, with element abundances within uncertainty of recommended values.

One hundred milligram powder aliquots for Sr and Nd isotope measurements were digested in the same manner as for trace element analyses and, after degradation of fluorides, equilibrated in 2.5 M HCl prior to a three-stage column procedure modified from Peters and Day (2017). The first column, using *BioRad* AG50-X8, was performed to separate Sr and major elements from the REE. The Sr cut was then purified using *Eichrom* Sr-specification resin prior to analysis by thermal ionization mass spectrometry (TIMS). The REE cut was further purified using *Eichrom* Ln-specification resin on homemade PTFE columns. Calibration of all sets of columns demonstrated 100% yield of Sr and Nd, with none remaining in the after cuts. Isotopic compositions of Sr and Nd were measured as metals in positive-ion mode on a *ThermoScientific* Triton Plus TIMS. Static measurements of strontium were corrected for mass fractionation using the exponential law and a reference $^{86}Sr/^{88}Sr$ value of 0.1194. Neodymium was measured dynamically in two steps, and mass fractionation corrected to $^{146}Nd/^{144}Nd = 0.7219$. Strontium blanks averaged 400 pg (<0.001% of loaded Sr) with measured $^{87}Sr/^{86}Sr$ of 0.7078. Neodymium blanks averaged 53 pg (<0.005% of loaded Nd) and could not be precisely analyzed for their $^{143}Nd/^{144}Nd$ ratios; consequently, the natural $^{143}Nd/^{144}Nd$ abundance of 0.5128 was used for blank corrections. Precision of isotopic measurements was monitored by repeated measurements of 300 ng NIST NBS987 (Sr) and 600 ng La Jolla (Nd) standard solutions, with results of 0.710243 ± 0.000014 ($n = 12$; 2 st. dev.) and 0.5118401 ± 0.0000010 ($n = 7$; 2 st. dev.), respectively. To assess the reproducibility of the Sr-Nd isotope method, aliquots of USGS basaltic reference materials, BHVO-2, BCR-2 and BIR-1 were measured, obtaining $^{87}Sr/^{86}Sr$ and $^{143}Nd/^{144}Nd$ within the range of previously reported values (Table S2: Raczek et al., 2003). Neodymium isotopes are reported as $\varepsilon_{Nd}i$, where $[(^{143}Nd/^{144}Nd)_{sample}/(^{143}Nd/^{144}Nd)_{CHUR})-1] \times 10{,}000$, at time of crystallization, where CHUR is the chondritic uniform reservoir value in the middle Miocene assuming modern day $^{143}Nd/^{144}Nd = 0.512638$ and $^{147}Sm/^{144}Nd = 0.1966$ (Hamilton et al., 1983).

Osmium isotope and HSE abundance analyses were performed on precisely weighed aliquots of homogenized powder that were then digested in sealed borosilicate Carius tubes with isotopically enriched multi-element spikes (^{99}Ru, ^{106}Pd, ^{185}Re, ^{190}Os, ^{191}Ir, ^{194}Pt), and 12 mL of a 1:2 mixture of multiply Teflon distilled HCl and HNO_3 purged of excess Os by repeated treatment and reaction with H_2O_2. Samples were digested to a maximum temperature of 270 °C in an oven for 72 h. Osmium was triply extracted from the acid using CCl_4 and then back extracted into HBr, prior to purification by micro-distillation. Rhenium and the other HSE were recovered and purified from the residual

solutions using standard anion exchange separation techniques (Day et al., 2016). Isotopic compositions of Os were measured in negative-ion mode using a *ThermoScientific* Triton TIMS in peak-jumping mode on the secondary electron multiplier. Rhenium, Pd, Pt, Ru and Ir were measured using a *Cetac Aridus* II desolvating nebuliser coupled to a *ThermoScientific* iCAPQc ICP-MS. Offline corrections for Os involved an oxide correction, an iterative fractionation correction using $^{192}Os/^{188}Os = 3.08271$ and assuming the exponential law, a ^{190}Os spike subtraction, and an Os blank subtraction. Precision for $^{187}Os/^{188}Os$, determined by repeated measurement of a 70 pg UMCP Johnson-Matthey standard solution was better than ±0.2% (2 SD; 0.11381 ± 12; $n = 12$). Rhenium, Ir, Pt, Pd and Ru isotopic ratios for sample solutions were corrected for mass fractionation using the deviation of the standard average run on the day over the natural ratio for the element. External reproducibility for HSE analyses was better than 0.5% for 0.5 ppb solutions and all reported values are blank corrected. The total procedural blanks ($n = 3$) run with the samples gave $^{187}Os/^{188}Os = 0.150 \pm 0.012$, with quantities (in picograms) of 2.5 [Re], 27 [Pd], 3.1 [Pt], 16 [Ru], 0.3 [Ir] and 0.3 [Os]. Blanks resulted in negligible corrections to samples (<5%) except for blank additions for Ru in CR1412, CR1516 and CR1517 (<10%) and Pd, Ru, Ir and Os in IM1505 and BCR-2 (10 to 34%; Table S3). Three basalt standards were analyzed with standards; a high-MgO picrite from the Canary Islands, 9C-TEN-05, a basalt from Kilauea (BHVO-2) and a basalt from the Columbia River (BCR-2), and results for these are consistent with prior work (Table S2; Fig. S2).

3. Results

Lower Steens Basalts (lower Steens B in Moore et al., 2018, 2020) have loss on ignition (LOI) averaging 4.7% and have sub-alkaline compositions with between 4.9 and 9 wt% MgO (average 7.5 wt%). Samples from the upper Steens Formation have lower LOI (~2.7%), alkaline basaltic compositions and generally lower MgO contents (5 to 9.3 wt%, average 6.6 wt%; Fig. S3). Compatible trace element concentrations tend to be higher in the lower (LS, $n = 12$) than in upper Steens Basalts (US, $n = 13$). Incompatible trace element contents show the opposite relationship, with the upper Steens Formation having more pronounced variations in Nb, Ta, Pb and Ti (Fig. S4). These are expressed by the different Nb* ($Nb/Nb^* = [Nb]_n/\sqrt{(([Th]_n \times [La]_n))}$, where n is the primitive mantle normalization; LS = 0.84 ± 0.05; US = 0.80 ± 0.13), Ta* ($Ta/Ta^* = [Nb]_n/\sqrt{(([Th]_n \times [La]_n))}$; LS = 0.91 ± 0.04; US = 0.85 ± 0.15) and Ti* ($Ti/Ti^* = [Ti]_n/\sqrt{(([Sm]_n \times [Tb]_n))}$; LS = 1.34 ± 0.04; US = 1.43 ± 0.10) for the sections, which in turn are less variable than in Imnaha ($n = 3$) and Pliocene ($n = 2$) basalts that were examined (together <0.6, <0.6 and > 1.65, respectively; Fig. S5). The studied samples generally compare well with previously reported data for the lower and upper Steens Formation (Johnson et al., 1998; Camp et al., 2013; Moore et al., 2018), with slightly higher MgO reported here for the upper Steens Formation. The presented samples are therefore representative of some of the most mafic lavas from the Steens Formation.

Lower Steens Basalts have $^{87}Sr/^{86}Sr$ from 0.70351 to 0.70361, and $^{143}Nd/^{144}Nd$ ranging from 0.51295 to 0.51296 ($\varepsilon_{Nd}i = +5.7$ to +5.9), which are similar to the range observed in the upper Steens Basalts ($^{87}Sr/^{86}Sr = 0.70339$ to 0.70362, $^{143}Nd/^{144}Nd = 0.51295$ to 0.51299, $\varepsilon_{Nd}i = +5.7$ to +6.5) (Table 1). These are some of the most depleted compositions measured for any CRBG lavas (Fig. 1), where the most MgO-rich basalts typically have the highest $\varepsilon_{Nd}i$ compositions.

Lower and upper Steens Basalts have fractionated primitive mantle normalized HSE patterns (Fig. 2) that are similar to those observed in magnesium basalts from other CFB (Rocha-Junior et al., 2012; Day et al., 2013; Peters and Day, 2017). Lower and upper Steens Basalts have similar Pd, Pt, Ru, Ir and Os contents, but upper Steens Basalts exhibit relatively elevated and more variable Re (Table 1). Lower and upper Steens Basalts have measured $^{187}Os/^{188}Os$ from 0.1296 to 0.1318 and 0.1292 to 0.1336, respectively. Age-corrected values reported relative to a chondritic composition ($\gamma Os = [(^{187}Os/^{188}Os)_{sample}/(^{187}Os/^{188}Os)_{chondrite})-1] \times 100$, at the time of crystallization)) are from +1.2 to +2.5 in lower Steens Basalts, but are more variable for upper Steens Basalts (+0.9 to −16), reflecting disturbance of Re in some samples since their eruption. Data reported in this study are similar to the five reported Re and Os abundances and $^{187}Os/^{188}Os$ given for the lower Steens Basalts by Moore et al. (2020), but do not extend to the low Os contents of their single upper Steens Formation sample. As observed by Moore et al. (2020), the Steens Basalts have generally higher Os contents for a given MgO content than other CFB (Fig. 3a). However, the Steens Basalts, and the most primitive basalts from the CRBG in general, have lower MgO contents and lower Os contents than in the most primitive lavas from other global CFB (Fig. 3a).

4. Discussion

4.1. Importance of crystallization and S-saturation in flood basalts

A notable feature of the CRBG are the consistently low MgO contents in lavas and intrusive dikes. The vast majority of lavas have MgO contents <7 wt% (e.g., Camp et al., 2013; Moore et al., 2018). In this respect, the CRBG is distinct other CFB, including Mesozoic examples such as the North Atlantic Igneous Province (NAIP), Deccan Traps, Parana-Etendeka or Karoo-Ferrar, where high magnesium basalts or picrites (>13.8 wt% MgO) can typically be found within the volcanic stratigraphies (e.g., Ellam et al., 1992; Schaefer et al., 2000; Stronik et al., 2017; Peters and Day, 2017), and the average MgO contents are higher (Moore et al., 2018, their Fig. 3). The earliest lavas of the CRBG are the Picture Gorge Basalts (Cahoon et al., 2020) and the Steens Basalts (Kasbohm and Schoene, 2018; Moore et al., 2018), yet the highest reported MgO contents of basalts from these formations rarely exceed 9 wt% MgO. Moore et al. (2018, 2020) have proposed, based on field observations, geochemical data, comparisons with mafic layered intrusions, and isotopic data that the Steens Basalts record temporary staging of parent melts at different levels within the crust where crystallization and incorporation of crustal melts, and scavenging of resultant cumulate materials took place. In particular, these authors recognized the high Os contents of the lower Steens Basalts for a given MgO content that they attributed to scavenging of Os-rich sulfides by recharge magmas passing through earlier (cumulate) crystallization products.

To assess magmatic processes acting on the HSE, fractional crystallization models were constructed whereby removal of a simple olivine-dominated cumulate leads to reduced MgO content in the residual melt. This model is coupled with S-saturation in the melt as a function of initial S content and decreasing MgO and, hence temperature. Parameters are identical to those used previously to model CFB lava compositions (Day, 2013) and are provided in Table S4 with results shown in Fig. 2. Despite parameter-dependence (e.g., silicate minerals in fractionating assemblage, MgO and S content of initial melt, FeS activity and partition coefficients into sulfide), these models reproduce the fractionation behavior of the HSE down to low-MgO basalts, not just for the Steens Basalts, but for global CFB (e.g., Day, 2013; Day et al., 2013). There is strong preference for Ru, Ir and Os (IPGE) relative to Pt, Pd and Re (PPGE) during fractional crystallization, requiring high sulfide-silicate melt partition coefficients for the IPGE relative to PPGE during basaltic magmatic evolution. These results support the separation of Os-, but also Ru- and Ir-rich alloys (e.g., Peregoedova et al., 2004), or sulfides (Moore et al., 2020), during fractional crystallization in staging melt reservoirs beneath the CRBG, even during the earliest phases of magmatism. The results also imply a parental magma with MgO contents much higher than basalts found in the field (>10 wt% MgO), supporting models of magma modification by crystallization and assimilation (e.g., Moore et al., 2018, 2020).

Significant HSE fractionation occurs in silicate melts due to the onset of sulfur saturation, which in ocean island basalts occurs at ~8 wt%

Table 1
Osmium, Sr and Nd isotope and highly siderophile element abundance data (in ppb) for Columbia River Flood Basalt lavas

Sample	Type	Height (m)	MgO (wt.%)	Re	Pd	Pt	Ru	Ir	Os	$^{187}Re/^{188}Os$	2σ	$^{187}Os/^{188}Os$	2σ	$\gamma_{Os}i$	$^{87}Sr/^{86}Sr$	2σ	$^{87}Sr/^{86}Sr_i$	$^{143}Nd/^{144}Nd$	2σ	$\varepsilon_{Nd}i$
CR1403	Pliocene Basalt	1706	7.1	4.248	0.604	0.400	0.441	0.429	0.118	173.6	2.6	0.13054	0.00046	0.1	0.703984	0.000002	0.70398	0.512833	0.000004	3.6
CR1404	Upper Steens	2136	6.3	1.550	9.547	7.602	0.566	0.364	0.119	62.8	0.9	0.13259	0.00013	-9.7						
CR1406	Upper Steens	2114	7.1	7.737	5.569	7.898	0.596	0.448	0.436	85.6	1.3	0.13111	0.00008	-16	0.703615	0.000002	0.70361	0.512954	0.000003	5.9
CR1407	Upper Steens	2104	8.5	3.029	6.783	8.159	0.699	0.421	0.568	25.7	0.4	0.13082	0.00007	-3.0	0.703481	0.000002	0.70347	0.512951	0.000003	5.8
CR1408	Upper Steens	2074	9.3	2.330	8.062	8.292	0.771	0.431	0.605	18.6	0.3	0.13132	0.00009	-1.0						
CR1411	Upper Steens	2082	7.5	2.657	8.962	9.764	0.778	0.305	0.639	20.0	0.3	0.12921	0.00015	-3.0	0.703415	0.000002	0.70340	0.512988	0.000003	6.5
Rpt	Upper Steens	2082	7.5	1.077	11.82	12.09	0.725	0.289	0.447	11.6	0.2	0.13190	0.00029	0.9	0.703415	0.000002	0.70340	0.512988	0.000003	6.5
CR1412	Upper Steens	2377	6.6	0.454	8.690	9.696	0.192	0.142	0.211	10.4	0.2	0.13362	0.00012	2.6						
CR1522	Upper Steens	2142	7.5	0.335	7.125	8.276	0.442	0.176	0.372	4.339	0.065	0.13321	0.00073	3.6	0.703481	0.000002	0.70347	0.512946	0.000003	5.7
CR1524	Upper Steens	2106	7.9	0.452	12.74	14.17	0.793	0.389	0.909	2.398	0.036	0.12983	0.00008	1.3	0.703390	0.000002	0.70337	0.512981	0.000003	6.4
CR1526	Lower Steens	2052	8.1	0.308	7.641	9.935	0.457	0.186	0.345	4.306	0.065	0.13184	0.00014	2.5						
CR1527	Lower Steens	2033	9.0	0.243	7.579	9.435	0.654	0.295	0.792	1.477	0.022	0.13021	0.00009	1.8	0.703611	0.000002	0.70360	0.512948	0.000003	5.7
CR1510	Lower Steens	1971	7.0	0.337	8.520	10.92	0.597	0.239	0.672	2.417	0.036	0.12983	0.00026	1.3	0.703508	0.000002	0.70350	0.512951	0.000002	5.8
CR1511	Lower Steens	1897	7.4	0.252	9.600	11.99	0.594	0.190	0.608	1.997	0.030	0.12956	0.00010	1.2						
CR1513	Lower Steens	1887	6.6												0.703548	0.000002	0.70348	0.512955	0.000002	5.9
CR1516	Lower Steens	1864	7.8	0.367	8.903	9.538	0.227	0.510	0.527	3.361	0.050	0.13163	0.00018	2.5	0.703512	0.000002	0.70349	0.512954	0.000003	5.9
Rpt	Lower Steens	1864	7.8												0.703507	0.000002	0.70349	0.512954	0.000003	5.9
CR1517	Lower Steens	1861	8.3	0.348	7.251	9.965	0.211	0.108	0.389	4.308	0.065	0.13107	0.00011	1.9						
CR1518	Lower Steens	1855	8.0	0.252	8.573	11.12	0.375	0.304	0.461	2.632	0.039	0.12997	0.00008	1.4						
CR1519A	Lower Steens	1841	7.3	0.273	7.758	10.50	0.515	0.305	0.698	1.884	0.028	0.13056	0.00012	2.0						
CR1530	Lower Steens	1900	7.6	0.199	7.370	10.41	0.376	0.293	0.469	2.043	0.031	0.13036	0.00011	1.8						
CR1531	Lower Steens	1896	7.4	0.226	8.911	10.59	0.444	0.372	0.568	1.92	0.03	0.13085	0.00014	2.2						
IM1505	Imnaha	-	5.1	0.380	0.170	0.248	0.164	0.012	0.030	61.9	0.9	0.28365	0.00062	109	0.703916	0.000002	0.70390	0.512834	0.000003	3.6

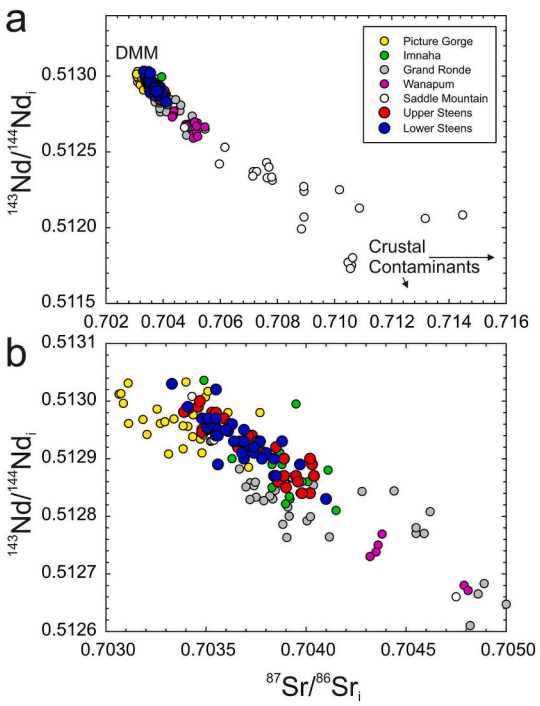

Fig. 1. Age-corrected (initial, i) $^{87}Sr/^{86}Sr$ versus $^{143}Nd/^{144}Nd$ for Steens Basalts from (a) this study and from Moore et al. (2020) versus other components of the Columbia River Basalt Group (CRBG; from compilation and references in Wolff et al., 2008) and, (b) an expanded view of the most depleted compositions in the CRBG. The compositions of melts from the depleted MORB mantle (DMM) and from crustal contaminants are shown in (a) and are identical to those from Wolff et al. (2008). Errors are smaller than symbols.

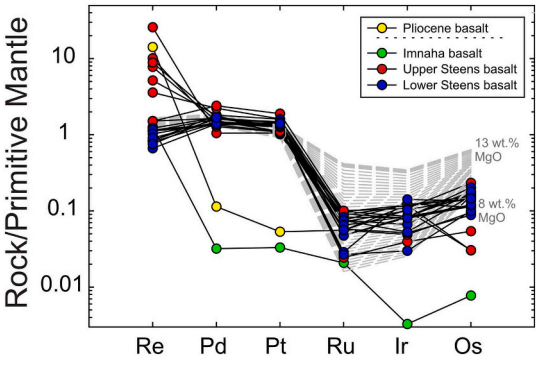

Fig. 2. Highly siderophile element systematics of the early Yellowstone mantle plume. Columbia River Basalt Group lavas from the earliest (Lower and upper Steens basalts) stages of volcanism are the most primitive samples with HSE patterns consistent with sulfide fractionation from a parental melt with MgO = 13 wt% (dashed lines, in 0.1% MgO increments), similar to that expected from ~10% partial melting of a fertile mantle source. Imnaha and Pliocene basalt compositions are consistent with formation from S-saturated melts. Model parameters are given in Table S4 and normalization is from Day et al. (2017).

MgO, and likely occurs at similar to higher MgO content in MORB (Day, 2013). Based on melt-inclusion S and FeO contents, lower Steens Basalts were S-undersaturated, while some upper Steens Basalts were likely S-saturated (Moore et al., 2020), with Grande Ronde basalts being pervasively S-saturated (Davis et al., 2017). The extent of S-saturation in CRBG lavas is consistent with HSE and MgO contents, where sharp decreases in Os, Ir and Ru contents do not occur until <7 wt% MgO, with Imnaha and Wanapum basalts having the lowest Os and MgO contents (Fig. 3a). Sulfide saturation at <7 wt% MgO is also supported by Cu

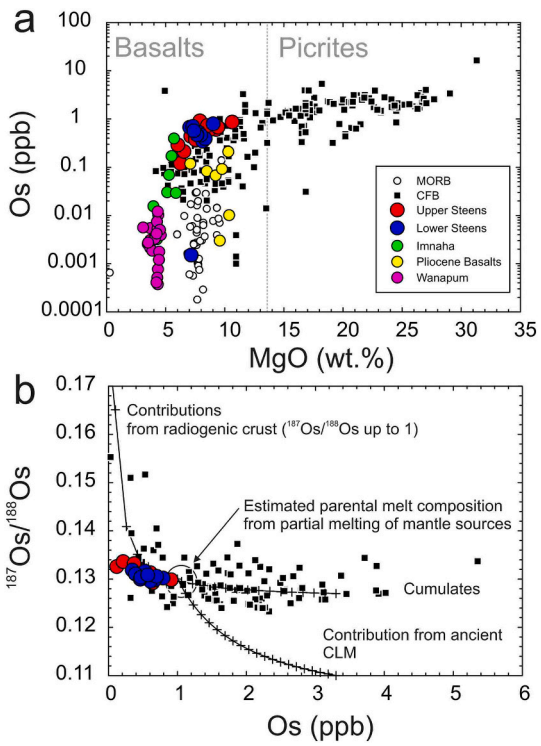

Fig. 3. Diagrams of (a) MgO versus Os for the Columbia River Basalt Group versus global CFB. (b) Osmium versus age-corrected $^{187}Os/^{188}Os$ for upper and lower Steens Basalts versus the global CFB compilation showing mixing lines (in 5% increments) between parental melts, crust and ancient continental lithospheric mantle as well as the trend of compositions in cumulates. Global compilation of CFB, mixing lines and reservoirs are from Day et al. (2013), with model parameters given in Table S5.

contents in the basalts, which broadly increase with decreasing MgO down to ~5 wt% MgO (Table S1). The effect of S-saturation and Os removal from melts explains the radically different Os isotopic compositions observed between the earlier Steens and Imnaha Basalts, versus Grande Ronde or Wanapum Basalts. With decreasing Os, melts become more susceptible to contamination from low Os crust. An alternative to scavenging of Os-rich sulfides by recharge magmas as proposed by Moore et al. (2020), therefore, is that S-saturation was generally not reached in CRBG magmas until <7 wt% MgO, in contrast to other CFB where S-saturation appears to have occurred at higher MgO contents. Possible causes of variable S-saturation at a given MgO content might include differing initial S contents in parental melts, or due to distinct staging, degassing, and crystallization processes during magma storage in the CRBG, relative to other CFB.

4.2. *Temporally variable crustal contributions to CRBG components*

Previous studies examining the Sr-Nd-(Hf-Pb) isotopic compositions of CRBG lavas have emphasized the important role of changing source contributions with time (e.g., Carlson et al., 1981; Brandon et al., 1993; Wolff et al., 2008; Moore et al., 2020). These studies have noted that there is an overall trend of more radiogenic $^{87}Sr/^{86}Sr$ and low $^{143}Nd/^{144}Nd$ that also correlates with age, in the order of the most depleted basaltic formations, including the Steens (~17 to 16.4 Ma) and the Picture Gorge Basalts (~17.2 to 16.1 Ma), to Imnaha (16.6 to 16.5 Ma), Grande Ronde (16.5 to 16.1 Ma), Wanapum (16.1 to 15.9 Ma) and, finally, the Saddle Mountains Basalts (<15.9 Ma) (Fig. 1, Fig. S6). These variations have been attributed to influences of enriched mantle sources (e.g., Carlson, 1984; Hooper and Hawkesworth, 1993; Camp and Hanan, 2008; Wolff et al., 2013), although crustal contamination is considered likely for the wider variations observed in Sr and Nd isotopes (Carlson,

1984; Wolff et al., 2008; Moore et al., 2020). These trends are also found in trace element compositions of lavas, with increasing negative Nb*, Ta* anomalies from the oldest to the youngest lavas, likely associated with increasing assimilation of Nb- and Ta-depleted arc-like terranes.

Osmium isotopes are a sensitive indicator of crustal contamination in CFB. During fractional crystallization of basaltic rocks, Os behaves compatibly, resulting in low Os contents in evolved melts (e.g., Day, 2013; Gannoun et al., 2016). Since potential crustal assimilants typically have low Os contents and radiogenic $^{187}Os/^{188}Os$, the effect is that more fractionated basaltic rocks become increasingly more susceptible to contamination by crust than more mafic magmas. Crustal contamination acting on CFB lavas have been spectacularly demonstrated by Re-Os isotope studies of Imnaha and Grande Ronde Basalts by Chesley and Ruiz (1998), and a Wanapum compound lava flow by Vye-Brown et al. (2013). Both studies analyzed rocks with relatively low MgO contents, and low Os (Fig. 3a) and reported more radiogenic $^{187}Os/^{188}Os$ than for the Steens Basalts studied here or in Moore et al. (2020). The Steens Basalts are some of the most primitive and high MgO basalts studied from the CRBG, and have initial Os isotope compositions consistent with originating from a primitive mantle like source (section 4.3). The lavas in the Steens Formation, however, tend to have lower $\varepsilon_{Nd}i$ with decreasing Os and MgO contents, and show slightly increasing $\gamma_{Os}i$ with decreasing MgO, suggestive of minor crustal contamination with time (Fig. 4).

Available Re-Os isotope data for the CRBG from Chesley and Ruiz (1998), Vye-Brown et al. (2013), Moore et al. (2020) and this study, represents perhaps the most comprehensive available for any CFB globally. With these data it is possible to assess first-order Os isotope variations with time assuming that the available data are broadly representative of the different basaltic formations. This approach is done acknowledging that, locally, crustal contamination - and crustal contaminants - likely vary substantially within lava flows. To overcome the issue of crustal contamination variations within and between lava flows, the large range in Re/Os for the low MgO basalts were utilized from younger formations to estimate compositions from errorchron initials, and the precise initial $^{187}Os/^{188}Os$ for the Steens Basalts was used to track changing compositions with time. The earliest studied and most MgO-rich lavas from the lower Steens Basalt have the least radiogenic $^{187}Os/^{188}Os$ ($\gamma_{Os}i = +1$), followed by the upper Steens Basalts (+3), Imnaha Basalts (+7), and then Grande Ronde (+89) and Wanapum (+90) (Fig. 5). Such variations, especially for the Grande Ronde and Wanapum Basalts, are impossible to explain by a changing mantle source composition, as no known mantle source could produce the basaltic compositions observed in the CRBG and also produce such radiogenic $^{187}Os/^{188}Os$. Instead, this variation reflects the increasing crustal contributions to CRBG lavas with time.

Increasingly radiogenic $^{187}Os/^{188}Os$ in CRBG lavas with time also correlates with increasing $^{87}Sr/^{86}Sr$, decreasing $^{143}Nd/^{144}Nd$, and a relationship of decreasing $\varepsilon_{Nd}i$ with decreasing MgO, as observed on a more local scale for the Steens Formation (Fig. 4). These geochemical signatures are typically considered as leading indicators of increasing crustal contributions to mantle-derived magmas. Taking average age-corrected Nd isotope variations for the different basalt formations (from Wolff et al., 2008; Moore et al., 2020; this study) it is possible to compare average Os-Nd isotopes compositions for components of the CRBG revealing the increasing contribution of crust and the strongly contaminated nature of Grande Ronde and Wanapum Basalts (Fig. 6). Although potential contaminants likely had variable incompatible trace element contents as well as a range of Nd isotope compositions, to simplify modelling we assumed that the major contaminants had Nd isotopic compositions from ancient crustal materials, consistent with the low $^{143}Nd/^{144}Nd$ and radiogenic $^{87}Sr/^{86}Sr$ observed in some CRBG lavas (Fig. 1). Osmium assimilation is assumed to involve isotopic compositions similar to average upper crustal compositions, where even relatively young, accreted terranes may have developed radiogenic $^{187}Os/^{188}Os$ (Table S5). Our models of crustal contamination for Os-Nd isotopes consider variable (0.05 to 1 ppb) Os contents due to S-saturation and reveal significantly less crustal contamination to the earlier Steens (1–2%) or Imnaha (~3%) Formation lavas than to later Grande Ronde (5–6%) or Wanapum Basalts (>6%; Figs. 6 and 7). In part, such differences likely reflect differential behavior of siderophile element (Os) budgets versus lithophile element (Sr-Nd-Pb) budgets during differentiation. Given the radiogenic Sr and low Nd isotope compositions of Saddle Mountain Basalts, a similar or higher level of crustal contamination is likely compared with Wanapum or Grande Ronde.

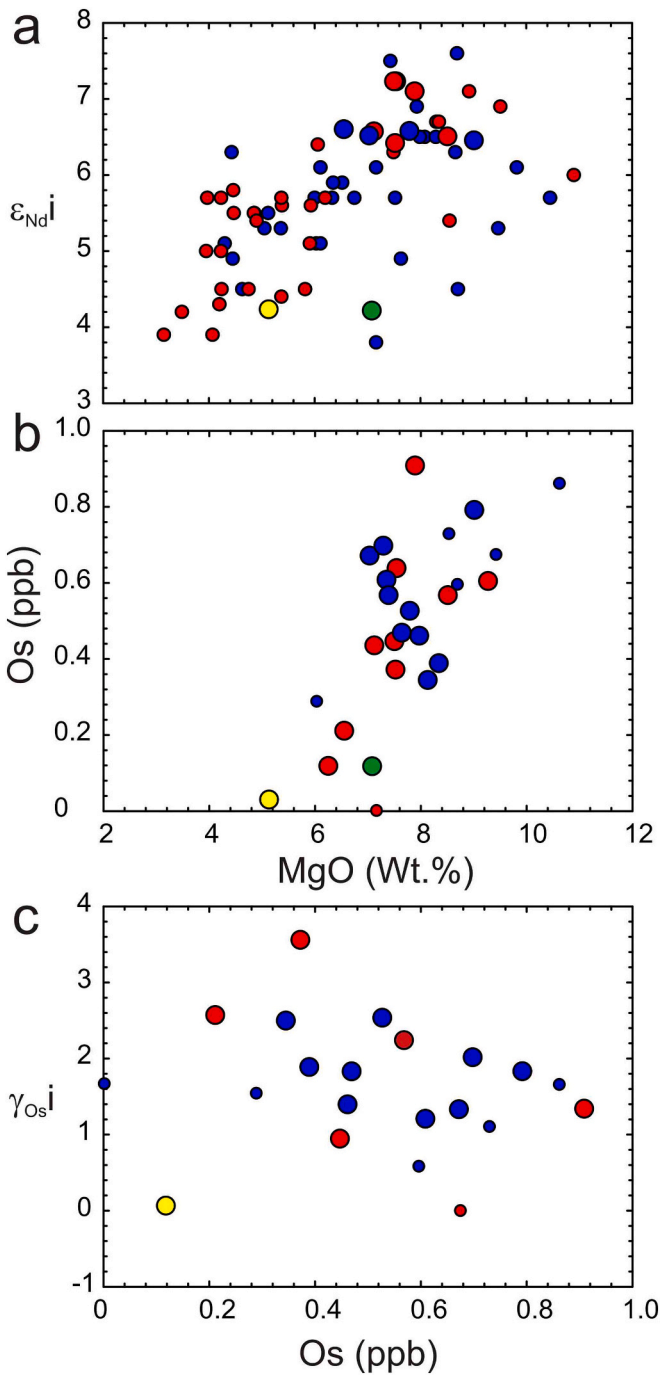

Fig. 4. MgO versus (a) initial $\varepsilon_{Nd}i$ and (b) Os contents, and Os contents versus initial $\gamma_{Os}i$ (c) for lower Steens (blue circles), upper Steens (red circles), and Imnaha Basalts (green circle) and a Pliocene basalt (yellow circle) from this study (large symbols) and Moore et al. (2020) (small symbols). Errors are generally smaller than symbols. (For interpretation of the references to colour in this figure legend, the reader is referred to the web version of this article.)

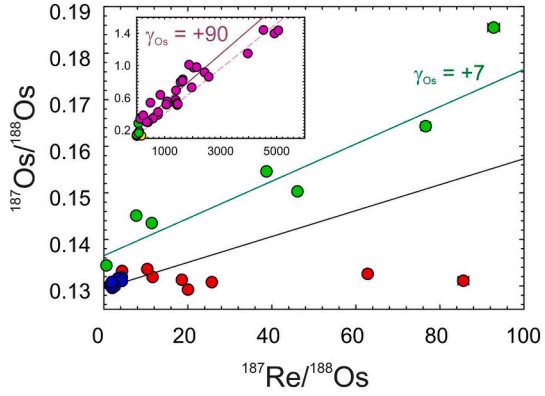

Fig. 5. Diagram of $^{187}Re/^{188}Os$ and $^{187}Os/^{188}Os$, expressed as γ_{Os} of lower Steens Basalts (+1; blue circles), upper Steens Basalts (+3; red circles) compared with later Imnaha (+7; green circles), Grande Ronde (+89, not visible, dashed line) and Wanapum Basalts (+90; pink circles). The black line denotes an isochron with an initial primitive mantle composition at 16.7 Ma. Wanapum, Grande Ronde and Imnaha data from Chesley and Ruiz (1998) and Vye-Brown et al. (2013). Errors are generally smaller than symbols. (For interpretation of the references to colour in this figure legend, the reader is referred to the web version of this article.)

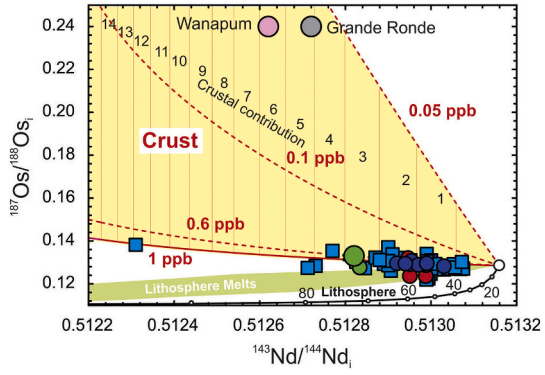

Fig. 6. Modification by crustal contamination in CRBG lavas (symbols are the same as for Fig. 2) versus North Atlantic Igneous Province picrite lavas (Light blue squares: NAIP; West Greenland and Baffin Island) as a function of models for crust contamination and interaction with lithosphere or lithosphere-derived melts (Table S5). Figure modified from Day (2013). (For interpretation of the references to colour in this figure legend, the reader is referred to the web version of this article.)

There are two major implications of this analysis. The first is that these estimates of crust are quite low and assimilation of this material alone cannot account for the range of MgO contents of CRBG lavas. Instead, they reinforce concepts that a significant fraction of the magmatic products that fed the CRBG are not at the surface. The generally low MgO contents of the lavas imply significant olivine ± pyroxene ± plagioclase and spinel fractionation accompanying this contamination indicating significant cumulate and intruded materials in the lithosphere (e.g., Moore et al., 2018). The second implication is that S-saturated lavas with low $^{143}Nd/^{144}Nd$ (i.e., Wanapum, Grande Ronde) could have come from parental melts with similar compositions to Imnaha or Steens Basalts. Consequently, all of the components of the CRBG could have originated from magmas with similar mantle source (s). The change from early-erupted S-undersaturated lavas with limited crustal contamination, to later-erupted S-saturated and strongly contaminated lavas is consistent with previous observations suggesting a changing magmatic plumbing system with time for the CRBG, possibly by sourcing of melts from the south, along the axis of the Yellowstone hotspot track (e.g., Wolff et al., 2008).

4.3. A primitive mantle-like source for the CRBG

Controversy has surrounded the likely mantle source of CRBG magmatism. After accounting for crustal contamination effects, numerous geochemical studies have argued for both enriched and depleted mantle components, including a Yellowstone mantle plume source, metasomatized lithospheric mantle or deep eclogitic crustal roots (Carlson, 1984; Hooper and Hawkesworth, 1993; Camp and Hanan, 2008; Wolff et al., 2008, 2013). An issue with determining the likely mantle source composition of the CRBG has been the lack of primitive basalts examined for Os isotope compositions. Results from this study, as well as from Moore et al. (2020), have shown that relatively MgO-rich and Os-rich lavas from the Steens Basalts of the CRBG have Os isotope compositions similar to those of a primitive mantle-type source, and that also have marginally higher Sr and lower Nd isotopic compositions compared with Pacific-type MORB. These compositions are similar to some of the most primitive basaltic rocks from other Mesozoic CFB (Ellam et al., 1992; (Horan et al., 1995) Schaefer et al., 2000; Peters and Day, 2017) and imply, like those locations, that there is a contribution from a primitive mantle source for the CRBG.

It is harder to examine the likelihood of contributions from distinct enriched and depleted mantle sources from Os isotopes in the CRBG, as has been suggested from Sr-Nd-Pb isotope variations in the Steens Basalts in particular (Carlson, 1984; Wolff et al., 2008; Camp et al., 2013; Moore et al., 2020). Contributions from such sources are possible, assuming that they lead to the Os isotope character recorded in the Steens Basalts. Based on the primitive mantle sources likely to have fed the CRBG, and evidence for a complex magmatic plumbing system in the crust, even at the inception of the earliest magmatism, it is also possible that the isotopic variations observed in CRBG lavas are entirely due to contamination of primitive mantle-derived melts by different crustal sources. For example, at least three major contaminants have been recognized, including arc-derived fluids (Brandon et al., 1993), Mesozoic accreted terranes that lie to the west of the Wyoming Craton, such as the Olds Ferry Terrane (Moore et al., 2020), or contamination by cratonic crust (Wolff et al., 2008). As noted previously, we assumed a singular crustal composition, but significant variation in composition may be inherited from variable contributions from these potential contaminants. From the most primitive lower Steens Basalts the likely mantle signature of CRBG magmatism and the ancestral Yellowstone hotspot track has $\varepsilon_{Nd}i \sim +6.5$, $^{87}Sr/^{86}Sr \sim 0.7033$ and $\gamma_{Os}i \sim +1$. Together with evidence for both high-$^{3}He/^{4}He$ today in Yellowstone (up to 24 R_A), in the Snake River Plain (up to 19 R_A; Graham et al., 2009), and in Imnaha basalts (at least up to 12 R_A; Dodson et al., 1997), these results implicate contributions from a mantle source distinct from the upper depleted mid-ocean ridge basalt mantle, which has marginally lower $^{187}Os/^{188}Os$, more depleted $^{143}Nd/^{144}Nd$ and lower $^{3}He/^{4}He$ (e.g., Day, 2013).

4.4. Geodynamic and climate implications during the Miocene

Observations of high-MgO basalts originating from a mantle plume source erupting early in the formation of the CRBG, and for progressively increasing crustal contamination with time have implications for both geodynamic models of the western margin of North America, and for linking the CRBG to climatic events during the mid-Miocene. In the case of geodynamic models, several have been proposed, especially focusing on the role of the Juan de Fuca plate, which has subducted under North America since the Mesozoic (Bunge and Grand, 2000), and likely affected initial CRBG eruption (Liu and Stegman, 2012). Two main classes of model have been proposed, namely formation of the CRBG in a back-arc like setting (e.g., Hart and Carlson, 1987; Christiansen et al., 2002), or lifting or tearing of the Juan de Fuca slab (Liu and Stegman, 2012; Coble and Mahood, 2012; Zhou et al., 2018). The former models possibly imply a slab contribution to magmas, and the latter models have explicitly argued for a slab contribution. The geochemical

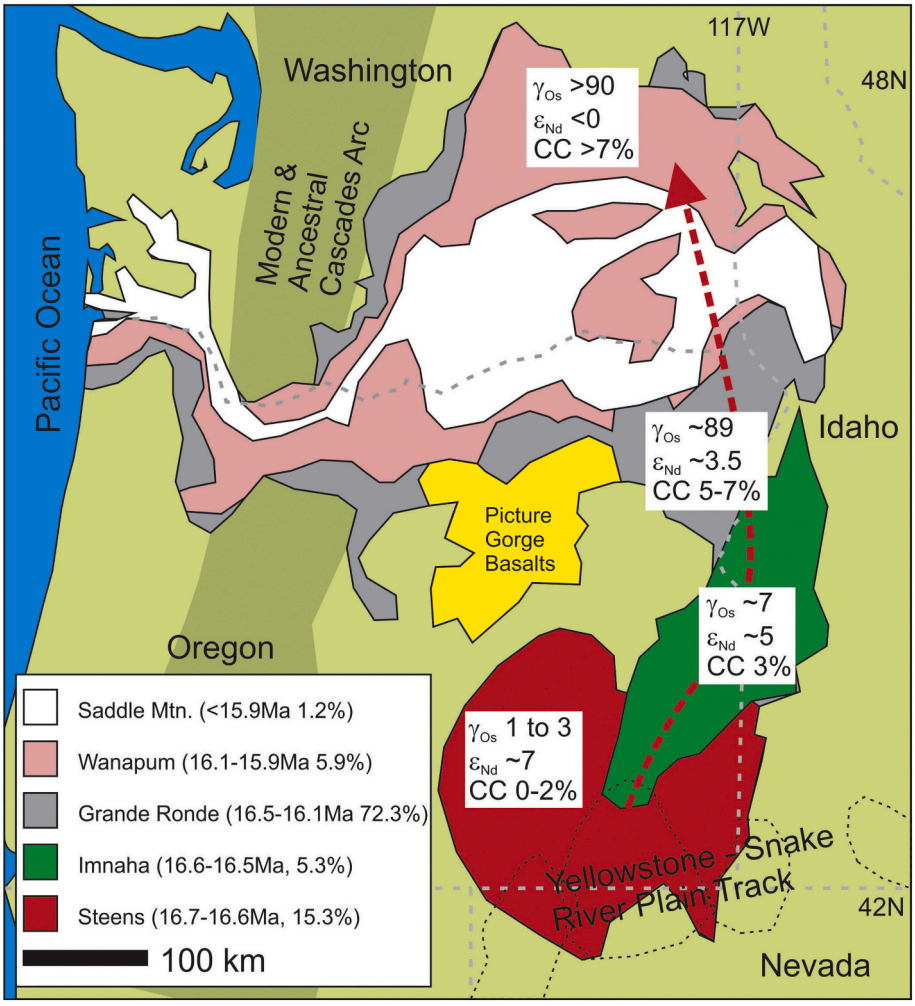

Fig. 7. Map of the region of the Columbia River Basalt Group showing the main units and their average Os and Nd isotope compositions and estimated crustal contributions (CC, after Fig. 6). The red dashed arrow shows the likely progression of volcanism with time, with the locus of magmatism beneath the Steens and Yellowstone-Snake River Plain track. (For interpretation of the references to colour in this figure legend, the reader is referred to the web version of this article.)

character of parental magmas to the Steens Basalts, and by implication from the crustal contamination models to the rest of the CRBG, do not provide evidence for a significant slab contribution, either from fluids, the oceanic crust, or the ocean lithosphere. This does not necessarily mean that contributions from such sources are not present, but that the signature of such sources cannot be readily distinguished from those of other CFB mantle sources, which do not require a slab input.

From an Os isotope perspective, assuming that all components of the CRBG were ultimately fed by magmas originating from the same mantle source that then experienced differential contamination within an evolving crustal magmatic plumbing system, then the quantities of crust can be related to temporal and volume estimates. The most up-to-date estimates for the CRBG (Reidel et al., 2013) indicate a total erupted volume of ~210,000 km^3, with roughly 15.3% represented by the Steens Basalts, erupted between ~17 to 16.4 Ma, 5.3% by Imnaha (16.6 to 16.5 Ma), 72.3% Grande Ronde (16.5 to 16.1 Ma), 5.9% by Wanapum (16.1 to 15.9 Ma) and finally 1.2% by the Saddle Mountains Basalts (<15.9 Ma). This most recent timescale for the CRBG, using both ^{40}Ar-^{39}Ar and U-Pb geochronology, indicates a protracted period of eruption spanning ~1.1 Ma (Kasbohm and Schoene, 2018), where nearly all of this temporal range captured within the Picture Gorge Basalts (Cahoon et al., 2020). Combining these volume estimates with the percentage estimates of crustal contamination from Os and Nd isotopes (section 4.2) and assuming that these crustal assimilation percentage estimates directly translate to total volumes without violating thermal constraints, then these indicate assimilation of 0 to ~600, 200 to 300, 7500 to 11,000, 850 to 1000 and 180 to 200 km^3 of crustal material to the Steens, Imnaha, Grande Ronde, Wanapum and Saddle Mountains Formations, respectively. From these calculations, out of the entire volume of erupted basalts in the CRBG approximately 4% (~8800 km^3) to 6% (13,000 km^3) could be entrained crustal material (Fig. 7). This estimate is only for volcanic rocks on the surface and it should be noted that total assimilation during CRBG magmatism is likely to have been several factors, to possibly an order of magnitude more than this, due to magmatism within the crust.

Crustal contamination has implications for linking the CRBG to the mid-Miocene Climatic Optimum (MCO). The MCO began around 17 Ma and ended around 15 Ma and was a period where atmospheric CO_2 (~350–400 ppm) was similar to today and sandwiched between periods with atmospheric CO_2 more similar to pre-industrial levels (200–260 ppm; Foster et al., 2012). This period was also marked by high-latitude sea surface temperatures, 4° to 6 °C above background temperature (Shevenell et al., 2004), a benthic δ^{18}O minimum, δ^{13}C maximum, and an ice sheet extent minimum. The CRBG has been linked to the MCO through excess release of CO_2 and other greenhouse gases during eruptions (e.g., Foster et al., 2012), that has been strengthened by the contracted geochronology for the CRBG (Kasbohm and Schoene, 2018). Armstrong-McKay et al. (2014) showed that the long-term carbon cycle of basalt degassing from the CRBG alone would have been negligible. However, 'cryptic degassing' and interaction with carbonaceous

sediments and crustal materials would have led to a total emission of 4090 to 5670 Pg of carbon with ~70% of this carbon emitted during the Grande Ronde Basalt eruptions. From these calculations, Armstrong-McKay et al. (2014) were able to reproduce the record of benthic $\delta^{13}C$ and atmospheric CO_2 change during the MCO. Using the estimated crustal assimilation volume estimates and assuming similar total CO_2 outputs does not drastically modify the conclusions of Armstrong-McKay et al. (2014), suggesting moderately greater contributions of CO_2 during the main phases of Grande Ronde eruption (3500 to 4700 Pg CO_2), and a low cryptic CO_2 addition from the Steens (0 to 250 Pg CO_2) and Imnaha (100 to 130 Pg CO_2) basalts.

Ultimately, estimates of CO_2 and other greenhouse gas outputs from the CRBG would be improved by detailed geochemical and geochronological analysis of the CRBG stratigraphy, as well as to identify and characterize likely crustal contaminants for $\delta^{13}C$ and total carbon and sulfur contents. Nonetheless, our results amplify the likelihood for the most significant cryptic (crustal) degassing occurring during the eruption of the Grande Ronde and Wanapum Basalts (16.5 to 15.9 Ma), rather than in the earliest periods of CRBG magmatism (Steens, Imnaha, Picture Gorge Basalts). Kasbohm and Schoene (2018) provided absolute chronology for the CRBG and noted a mismatch between its onset and the beginning of the MCO. They suggest that either the events were unrelated or that further work to refine age models for climate proxy records across the MCO and investigations of rates of eruptions for the CRBG may be required before a link could be determined. The evidence for the most extensive crustal interaction with mantle-derived melts occurring after ~16.5 Ma, that may also be coupled to cryptic degassing, suggests that a link between the onset of the MCO and CRBG is tenuous. Instead, the CRBG may have had a strong contributing impact to an ongoing climatic warming event, rather than being the trigger for it.

5. Conclusions

Comprehensive examination of Steens Basalts for Os-Sr-Nd isotopes and highly siderophile element abundances confirms that they are some of the highest MgO and most primitive basalts from the Columbia River Basalt Group (CRBG). Lower and upper Steens Basalts originate from a primitive mantle source ($\varepsilon_{Nd}i = +6.5$, $^{87}Sr/^{86}Sr = 0.7033$; $^{187}Os/^{188}Os = 0.129$). These primary magma compositions for the Steens basalts do not provide compelling evidence for a subducted slab component, instead suggesting inception from primitive mantle sources more similar to the mantle sources of other Mesozoic continental flood basalts (CFB; e.g., Deccan, North Atlantic Igneous Province). Onset of sulfide saturation in the CRBG occured at lower MgO (<7 wt%) than in other CFB (~ 8 wt%) leading to the high Os contents in Steens basalts. Collectively, Steens basalts exhibit decreasing Os contents, $\varepsilon_{Nd}i$ values and increasing $^{187}Os/^{188}Os$ with decreasing MgO. These geochemical signatures are consistent with increasing crustal contamination to parent melts with time, a feature that is also shared for the CRBG as a whole. Calculations of the mantle and crust components to the different basalt formations of the CRBG indicates that between 4 and 6% of their total mass is derived from assimilation of crust. The major phases of eruption of crustally contaminated basalts occurred after 16.5 Ma, when Grande Ronde and Wanapum lavas were emplaced. The earlier Steens and Imnaha Basalts show far more limited crustal contamination. Equating the crustal contamination to additional CO_2 suggests that the onset of mid-Miocene Climatic Optimum preceded CRBG magmatism. This would indicate that eruption of CRBG was a contributing factor to climate change at that time but was not the trigger for it.

Declaration of Competing Interest

The authors declare no conflicts of interest.

Acknowledgements

Financial support to complete this work came from the NSF EAR program (EAR-1447130; EAR 1918322) and the National Geographic Society (GEFNE28-11) to JMDD. BJPs participation was partly supported by the SNSF *Ambizione* program (PZ00P2_186064). We are grateful to Jasmeet Dhaliwal, Shi Sim and Diana Brown for assistance with sample collection, and to Nicole Moore for discussions. Nicole Moore and John Wolff are thanked for their helpful reviews.

Appendix A. Supplementary data

Supplementary data to this article can be found online at https://doi.org/10.1016/j.chemgeo.2021.120197.

References

Armstrong-McKay, D.I., Tyrrell, T., Wilson, P.A., Foster, G.L., 2014. Estimating the impact of the cryptic degassing of large Igneous Provinces: a mid-miocene case-study. Earth Planet. Sci. Lett. 403, 254–262.
Barry, T.L., Kelley, S.P., Reidel, S.P., Camp, V.E., Self, S., Jarboe, N.A., Duncan, R.A., Renne, P.R., Ross, M.E., Wolff, J.A., 2013. Eruption Chronology of the Columbia River Basalt Group. The Columbia River Flood Basalt Province: Geological Society of America Special Paper, 497, pp. 45–66.
Boyd, F.R., Mertzman, S.A., 1987. Composition and structure of the Kaapvaal lithosphere, southern Africa. In: Mysen, B.O. (Ed.), Magmatic Processes: Physicochemical Principles, 1. Geochemical Society Special Publications, pp. 13–24.
Brandon, A.D., Hooper, P.R., Goles, G.G., Lambert, R.S.J., 1993. Evaluating crustal contamination in continental basalts: the isotopic composition of the Picture Gorge Basalt of the Columbia River Basalt Group. Contrib. Mineral. Petrol. 114, 452–464.
Bunge, H.-P., Grand, S.P., 2000. Mesozoic plate-motion history below the Northeast Pacific Ocean from seismic images of the subducted Farallon slab. Nature 405, 337–340.
Cahoon, E.B., Streck, M.J., Koppers, A.A., Miggins, D.P., 2020. Reshuffling the Columbia River Basalt chronology—Picture Gorge Basalt, the earliest-and longest-erupting formation. Geology 48, 348–352.
Camp, V.E., Hanan, B.B., 2008. A plume-triggered delamination origin for the Columbia River Basalt Group. Geosphere 4 (3), 480–495.
Camp, V.E., Ross, M.E., Duncan, R.A., Jarboe, N.A., Coe, R.S., Hanan, B.B., Johnson, J.A., Reidel, S.P., 2013. The Steens Basalt: Earliest Lavas of the Columbia River Basalt Group. The Columbia River Flood Basalt Province: Geological Society of America Special Paper, 497, pp. 87–116.
Carlson, R.W., 1984. Isotopic constraints on Columbia River flood basalt genesis and the nature of the subcontinental mantle. Geochim. Cosmochim. Acta 48, 2357–2372.
Carlson, R.W., Lugmair, G.W., Macdougall, J.D., 1981. Crustal influence in the generation of continental flood basalts. Nature 289, 160–162.
Chesley, J.T., Ruiz, J., 1998. Crust-mantle interaction in large igneous provinces: implications from Re-Os isotope systematics of the Columbia River flood basalts. Earth Planet. Sci. Lett. 154, 1–11.
Christiansen, R.L., Foulger, G.R., Evans, J.R., 2002. Upper-mantle origin of the Yellowstone hotspot. Geol. Soc. Am. Bull. 114, 1245–1256.
Coble, M.A., Mahood, G.A., 2012. Initial impingement of the Yellowstone plume located by widespread silicic volcanism contemporaneous with Columbia River flood basalts. Geology 40, 655–658.
Coffin, M.F., Eldholm, O., 1994. Large igneous provinces: Crustal structure, dimensions, and external consequences. Rev. Geophys. 32, 1–36.
Courtillot, V.E., Renne, P.R., 2003. On the ages of flood basalt events. Compt. Rendus Geosci. 335, 113–140.
Davis, K.N., Wolff, J.A., Rowe, M.C., Neill, O.K., 2017. Sulfur release from main-phase Columbia River Basalt eruptions. Geology 45, 1043–1046.
Day, J.M.D., 2013. Hotspot volcanism and highly siderophile elements. Chem. Geol. 341, 50–74.
Day, J.M.D., Pearson, D.G., Hulbert, L.J., 2013. Highly siderophile element behaviour during flood basalt genesis and evidence for melts from intrusive chromitite formation in the Mackenzie large igneous province. Lithos 182, 242–258.
Day, J.M.D., Waters, C.L., Schaefer, B.F., Walker, R.J., Turner, S., 2016. Use of hydrofluoric acid desilicification in the determination of highly siderophile element abundances and Re-Pt-Os isotope systematics in mafic-ultramafic rocks. Geostand. Geoanal. Res. 40, 49–65.
Day, J.M.D., Walker, R.J., Warren, J.M., 2017. ^{186}Os-^{187}Os and highly siderophile element abundance systematics of the mantle revealed by abyssal peridotites and Os-rich alloys. Geochim. Cosmochim. Acta 200, 232–254.
Dodson, A., Kennedy, B.M., DePaolo, D.J., 1997. Helium and neon isotopes in the Imnaha Basalt, Columbia River Basalt Group: evidence for a Yellowstone plume source. Earth Planet. Sci. Lett. 150, 443–451.
Ellam, R.M., Carlson, R.W., Shirey, S.B., 1992. Evidence from Re-Os isotopes for plume-lithosphere mixing in Karoo flood basalt genesis. Nature 359, 718–721.
Foster, G.L., Lear, C.H., Rae, J.W., 2012. The evolution of pCO_2, ice volume and climate during the middle Miocene. Earth Planet. Sci. Lett. 341, 243–254.
Gannoun, A., Burton, K.W., Day, J.M.D., Harvey, J., Schiano, P., Parkinson, I., 2016. Highly siderophile element and Os Isotope Systematics of volcanic rocks at divergent

and convergent plate boundaries and in intraplate settings. Rev. Mineral. Geochem. 81, 651–724.
Graham, D.W., Reid, M.R., Jordan, B.T., Grunder, A.L., Leeman, W.P., Lupton, J.E., 2009. Mantle source provinces beneath the northwestern USA delimited by helium isotopes in young basalts. J. Volcanol. Geotherm. Res. 188, 128–140.
Hamilton, P.J., O'Nions, R.K., Bridgwater, D., Nutman, A., 1983. Sm-Nd studies of Archean metasediments and metavolcanics from West Greenland and their implications for the Earth's early history. Earth Planet. Sci. Lett. 62, 263–272.
Hart, W.K., Carlson, R.W., 1987. Tectonic controls on magma genesis and evolution in the northwestern United States. J. Volcan. Geotherm. Res. 32, 119–135.
Hooper, P.R., Hawkesworth, C.J., 1993. Isotopic and geochemical constraints on the origin and evolution of the Columbia River basalt. J. Petrol. 34, 1203–1246.
Horan, M.F., Walker, R.J., Fedorenko, V.A., Czamanske, G.K., 1995. Osmium and neodymium isotopic constraints on the temporal and spatial evolution of Siberian flood basalt sources. Geochim. Cosmochim. Acta 59 (24), 5159–5168.
Johnson, J.A., Hawkesworth, C.J., Hooper, P.R., Binger, G.B., 1998. Major-and Trace-Element Analyses of Steens Basalt, southeastern Oregon. US Geological Survey, pp. 98–482.
Kasbohm, J., Schoene, B., 2018. Rapid eruption of the Columbia River flood basalt and correlation with the mid-Miocene climate optimum. Sci. Adv. 4 (9) (p.eaat8223).
Liu, L., Stegman, D.R., 2012. Origin of Columbia River flood basalt controlled by propagating rupture of the Farallon slab. Nature 482, 386–389.
Moore, N.E., Grunder, A.L., Bohrson, W.A., 2018. The three-stage petrochemical evolution of the Steens Basalt (Southeast Oregon, USA) compared to large igneous provinces and layered mafic intrusions. Geosphere 14 (6), 2505–2532.
Moore, N.E., Grunder, A.L., Bohrson, W.A., Carlson, R.W., Bindeman, I.N., 2020. Changing mantle sources and the effects of crustal passage on the Steens Basalt, SE Oregon: Chemical and isotopic constraints. Geochem. Geophys. Geosyst. 21 (8) (p. e2020GC008910).
Peregoedova, A., Barnes, S.-J., Baker, D.R., 2004. The formation of Pt–Ir alloys and Cu–Pd-rich sulfide melts by partial desulfurization of Fe–Ni–Cu sulfides: results of experiments and implications for natural systems. Chem. Geol. 208, 247–264.
Pernet-Fisher, J.F., Day, J.M.D., Howarth, G.H., Ryabov, V.V., Taylor, L.A., 2017. Atmospheric outgassing and native-iron formation during carbonaceous sediment–basalt melt interactions. Earth Planet. Sci. Lett. 460, 201–212.
Peters, B.J., Day, J.M.D., 2017. A geochemical link between plume head and tail volcanism. Geochem. Perspect. Lett. 5, 29–34.
Raczek, I., Jochum, K.P., Hofmann, A.W., 2003. Neodymium and strontium isotope data for USGS reference materials BCR-1, BCR-2, BHVO-1, BHVO-2, AGV-1, AGV-2, GSP-1, GSP-2 and eight MPI-DING reference glasses. Geostand. Newslett. 27, 173–179.
Rampino, M.R., Self, S., Sigurdsson, H., 2015. Large igneous provinces and biotic extinctions. In: Houghton, B., McNutt, S., Rymer, H., Stix, J. (Eds.), The Encyclopedia of Volcanoes. Elsevier, pp. 1049–1058.
Reidel, S.P., Camp, V.E., Ross, M.E., Tolan, T.L., Marton, B.S., 2013. The Columbia River flood basalt province: Stratigraphy, areal extent, volume, and physical volcanology. Geol. Soc. Am. Spec. Pap. 497, 1–39.
Rocha-Junior, E.R.V., Puchtel, I.S., Marques, L.S., Walker, R.J., Machado, F.B., Nardy, A. J.R., Babinski, M., Figueiredo, A.M.G., 2012. Re-Os isotope and highly siderophile element systematics of the Parana continental flood basalts (Brazil). Earth Planet. Sci. Lett. 337-338, 164–173.
Schaefer, B.F., Parkinson, I.J., Hawkesworth, C.J., 2000. Deep mantle plume osmium isotope signature from West Greenland Tertiary picrites. Earth Planet. Sci. Lett. 175, 105–118.
Self, S., Widdowson, M., Thordarson, T., Jay, A.E., 2006. Volatile fluxes during flood basalt eruptions and potential effects on the global environment: A Deccan perspective. Earth Planet. Sci. Lett. 248, 518–532.
Shevenell, A.E., Kennett, J.P., Lea, D.W., 2004. Middle Miocene Southern Ocean cooling and Antarctic cryosphere expansion. Science 305, 1766–1770.
Shirey, S.B., Walker, R.J., 1998. The Re-Os isotope system in cosmochemistry and high-temperature geochemistry. Annu. Rev. Earth Planet. Sci. 26, 423–500.
Stronik, N.A., Krienitz, M.-S., Niedermann, S., Romer, R.L., Harris, C., Trumbull, R.B., Day, J.M.D., 2017. Helium isotope evidence for a deep-seated mantle plume involved in South Atlantic break-up. Geology 45, 827–830.
Vye-Brown, C., Gannoun, A., Barry, T.L., Self, S., Burton, K.W., 2013. Osmium isotope variations accompanying the eruption of a single lava flow field in the Columbia River Flood Basalt Province. Earth Planet. Sci. Lett. 368, 183–194.
Walker, G.W., 1990. Miocene and younger rocks of the Blue Mountains region, exclusive of the Columbia River Basalt Group and associated mafic lava flows: U.S. Geol. Surv. Prof. Pap. 1437, 101–118.
Wolff, J.A., Ramos, F.C., Hart, G.L., Patterson, J.D., Brandon, A.D., 2008. Columbia River flood basalts from a centralized crustal magmatic system. Nat. Geosci. 1, 177–180.
Wolff, J.A., Ramos, F.C., Reidel, S.P., Camp, V.E., Ross, M.E., Martin, B.S., Tolan, T.L., Wells, R.E., 2013. Source materials for the main phase of the Columbia River Basalt Group: Geochemical evidence and implications for magma storage and transport. In: The Columbia River Flood Basalt Province: Geological Society of America Special Paper, 497, pp. 273–291.
Zhou, Q., Liu, L., Hu, J., 2018. Western US volcanism due to intruding oceanic mantle driven by ancient Farallon slabs. Nat. Geosci. 11, 70–76.